Electronic Supplementary Material (ESI) for Chemical Science.

Supporting Information

Triplet energy transfer from quantum dots increases Ln(III) photoluminescence, enabling excitation at visible wavelengths

Tingting Huang‡[a], Sheng He‡[b], Anji Ni [b], Tianquan Lian*[b], and Ming Lee Tang*[a]

[a]Department of Chemistry, University of Utah, Salt Lake City, UT, 84112, United States.
[b] Department of Chemistry, Emory University, 1515 Dickey Drive Northeast, Atlanta, Georgia 30322, USA
‡ T.H. and S.H contributed equally to this paper

1. Instrumentation.

Linear absorption spectra were recorded on a Cary 5000 UV-Vis absorption spectrophotometer. 405nm laser excited photoluminescence spectra were recorded at right angles to the excitation with an Oxford Instruments Andor KYMERA-328i-B2 spectrometer, 150 l/mm grating and a DU401A-BVF silicon iDus camera. The samples are prepared in airtight Starna cuvettes with screw tops in a nitrogen glove box. Photoluminescence was also recorded with Horiba FluoroMax 4-C-SP spectrometer. The photoluminescence quantum yields were calculated with 4-(Dicyanomethylene)-2-methyl-6-(4-dimethylaminostyryl)-4H-pyran (DCM) reference excited with a 405 nm laser (OBIS). Photoluminescence spectra with other wavelengths excitation were recorded on Horiba FluoroMax 4-C-SP spectrometer.

Femtosecond TA setup. In the femtosecond TA experiments, we used a regenerative amplified Ti: Sapphire femtosecond laser system (Astrella, Coherent) to generate the 800 nm fundamental pulse (1 kHz repetition rate, 35 fs pulse duration, and 5.1 mJ/pulse), which was split by a 90:10 beam splitter. The 10% 800 nm fundamental pulse went through a delay stage (with a maximum delay time of 8 ns) in the Helios system (Ultrafast System LLC) and was then attenuated by a neutral-density filter before it was focused on a sapphire to generate a white light continuum (WLC, from 420 nm to 780 nm) probe pulse. The WLC was focused on the sample to monitor the absorbance change. For the 90 % fundamental beam, half of it was used to pump a visible optical parameter amplifier (OPA, Light Conversion LLC) to generate the pump pulse with desired wavelength in the visible range. For the 400 nm pump pulse, the 800 nm fundamental pulse was frequency-doubled by a BBO crystal. The output pump pulse was then split by a 50:50 beam splitter. The reflected half was guided into the nanosecond TA setup, as discussed below. The transmitted half was directed into the Helios system and then modulated by a 500 Hz chopper before it was focused on the sample. The power of the pump pulse was controlled by a series of neutral-density filters. The data collection was completed in the Helios system (Ultrafast System LLC), with an instrument response function (IRF) of 70 fs. All samples were contained in 1 mm thick quartz cuvettes and were constantly stirred. All measurements were conducted at room temperature under air-free environment. The sample optical densities at the excitation wavelength are about 0.2.

Nanosecond TA setup. Nanosecond TA was performed with the EOS spectrometer (Ultrafast Systems LLC). The pump beam was generated by the same OPA used in the femtosecond TA setup. A supercontinuum laser (Disco-2-UV, Leukos) was use as the WLC probe. The WLC was split to a probe beam and a reference beam, which were then focused into a fiber-coupled multichannel spectrometer with complementary metal-oxide-semiconductor (CMOS) sensors. The function of this reference beam was to account for the pulse-to-pulse fluctuation of the WLC. The delay time between the pump and probe beam was controlled by a digital delay generator (CNT-90, Pendulum Instruments). The IRF of this system was measured to be 400 ps.

2. Experimental section.

2.1 Chemicals

Cadmium oxide (CdO, 99.999%) was purchased from TCI America; Sulfur powder (99%+) purchased from Strem. Oleic acid (OA, tech. grade, 90%),1-octadecene (ODE, 90%), Europium tris[3-(trifluoromethylhydroxymethylene)-(+)-camphorate] (Eu{(+)-facam}$_3$), 4-(dicyanomethylene)-2-methyl-6-(4-dimethylaminostyryl)-4H-pyran (DCM) were purchased from Sigma Aldrich. 1-Napthoic acid (98%) was purchased from Thermo Scientific. All molecules were used as received. Dry and degassed toluene and THF were obtained from the MBraun solvent purification system.

2.2 Synthesis of CdS QDs

CdS QDs were synthesized and purified based on the procedure by Peng in Angew. Chem. Int. Ed. 2002, 41, 2368-2371. CdO 257 mg (2 mmol), 6 ml Oleic Acid and 15.8 ml ODE was mixed in a 50 ml, three-necked flask equipped with a condenser and temperature controller. The reaction mixture was evacuated for 1 hour at 110°C. The mixture is then stirred and heated to 260°C under nitrogen until it turns clear. 32 mg of sulfur powder in 3 ml ODE is prepared in a glovebox and sonicated. The sulfur precursor is injected to the reaction mixture, time and temperature varied from 200–220 °C to achieve CdS QDs of suitable size. The surface of as-synthesized QDs is capped with oleic acid ligands.

CdS Size[a)]	**Absorption maximum**[b)] **[nm]**	**Absorption FWHM**[c)] **[nm]**	**PL maximum**[d)] **[nm]**	**CdS PLQY**[e)] **[%]**
CdS 405nm	405	22	426	0.11
CdS 416nm	416	22	442	1.96
CdS 435nm	435	24	449	1.86
CdS 439nm	439	24	454	6.63
CdS 445nm	445	22	464	0.54

Table S1. a) QDs denoted by absorption maximum, b) Absorption peak position, c) Absorption Full width at half maximum, d) PL maximum position, e) PLQY of all CdS in toluene, R.T. With excitation at 405nm or at CdS band-edge

2.3 Ligand exchanged with 1–NCA and sample preparation:

For CdS and 1–NCA ligand exchange experiments, CdS in toluene stock solution was added to 7.5 mM 1–NCA ligands in toluene under nitrogen atmosphere glovebox (MBraun). The concentration of 1–NCA was fine tuned to give the highest PLQY of the Eu{(+)-facam}$_3$ emitter, as detailed in Figure S1. This mixture was stirred vigorously overnight. For CdSe and 9–ACA ligand exchange, 524 nm size CdSe in toluene stock solution is added to 1.91 mM 9–ACA ligands saturated solution in toluene under nitrogen. In the final 1cm cuvette, the OD@405nm =0.542 and the OD@524nm =0.492. Steady state PL measurements were performed. All experiments were strictly air free, with samples made inside a glove box and kept in the dark, in airtight fluorescence cuvettes during the entire experimental period.

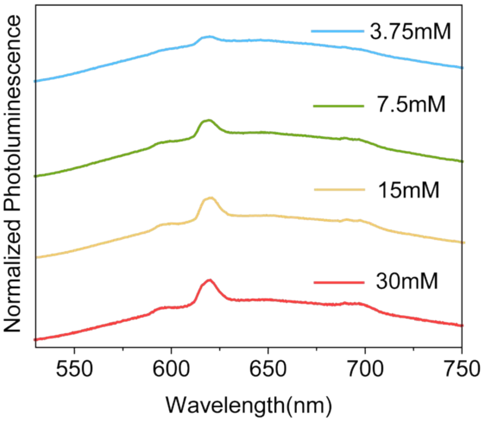

Figure S1. Normalized PL of Eu{(+)-facam}$_3$ in the CdS/1–NCA toluene solutions, with the 1–NCA concentration of 3.75 mM, 7.5 mM, 15 mM and 30 mM, R.T. The broad baseline is due to the trapped exciton emission in CdS QDs as in Figure S3. At 1–NCA concentrations exceeding 7.5 mM, the photoluminescence quantum yield (PLQY) from the Eu{(+)-facam}$_3$ emitter stopped increasing, hence 7.5 mM of 1–NCA was used for the spectroscopy studies in the main text.

Then, a concentrated Eu{(+)-facam}$_3$ emitter stock solution in toluene was added to CdS/1–NCA solution to give a final Eu{(+)-facam}$_3$ concentration of 1.23 mM in CdS/1–NCA toluene solution. The final QD concentration was 2.5–9.9 × 10^{-1} μM. At this micromolar concentrations, the QDs capped with native oleic acid ligands remain soluble in toluene. The samples were loaded into 1 cm pathlength air free quartz cuvette in glove box. The electronic absorption spectra was observed by using the Cary 5000. The CdS absorption at 405 nm and band edge are listed in Table S2. The CdS optical density at 405 nm or its band-edge is ~0.2–0.5.

CdS Absorption maximum	CdS Contribution O.D.	
	at 405 nm	at band edge
CdS 405 nm	0.237	0.237
CdS 416 nm	0.295	0.496
CdS 435 nm	0.344	0.391
CdS 439 nm	0.196	0.199
CdS 445 nm	0.472	0.440

Table S2. The CdS OD in the 1 cm cuvette after ligand exchange, in 1.23 mM Eu{(+)-facam}$_3$ in toluene R.T.

2.4 Quantum yield measurements and calculations

2.4.1 Eu{(+)-facam}$_3$ PL measurements with CdS and 1–NCA ligand

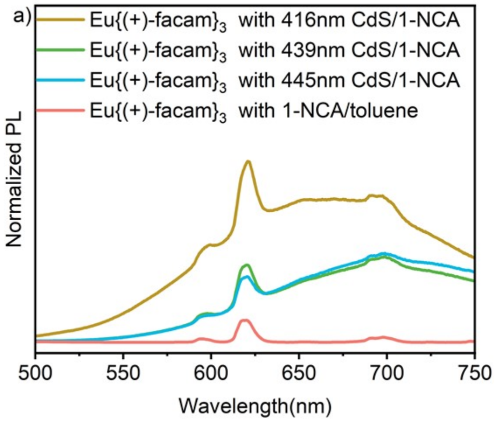

Figure S2. Photoluminescence spectra with excitation at 405 nm showing the CdS trap state emission.

2.4.2 Excitation at 405nm discussion regarding Eu{(+)-facam}$_3$ absorption.

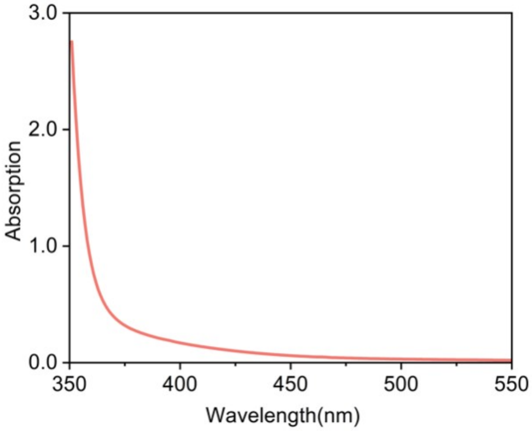

Figure S3. Absorption tail after 400 nm of 1.23 mM Eu{(+)-facam}$_3$ in 1–NCA/toluene solution, R.T.

Fig. S3 shows that this extremely concentrated solution has an absorption tail that extends to 500nm, even though the diluted Eu{(+)-facam}$_3$ and 1-NCA molecules individually dissolved in toluene do not absorb beyond 350 nm and 450 nm respectively, as shown in Fig. 1b. In this work, CdS QDs of different sizes when functionalized with 1-NCA to give CdS/1-NCA and mixed with 1.23mM Eu{(+)-facam}$_3$, then excited both at 405 nm and at the QD band edge (absorption maxima). As shown in Fig. 2c, with 405 nm excitation, the Eu(III) PL was only enhanced 2−6.6 fold. However, with excitation at the QD band edge, the Eu(III) PL is enhanced 5.8−21.4 fold. This is because the QD absorbs significantly more photons at its bandedge compared to the Eu{(+)-facam}$_3$ molecule. However, as the QD size increases, the driving force for triplet energy transfer decreases, and the enhancement in Eu(III) PL is less significant. Thus, the largest enhancement occurs for mid-sized QDs absorbing maximally at 435 nm.

2.4.3 Eu{(+)-facam}$_3$ PL quantum yield calculation

$$\Phi_{sample} = \Phi_{DCM} * \frac{n_{sample}^{2}}{n_{DCM}^{2}} * \frac{1-10^{-A_{DCM}}}{1-10^{-A_{sample}}} * \frac{[Area]_{sample}}{[Area]_{DCM}} \qquad \text{(Eq. S1)}$$

Φ_{DCM} is the quantum yield of 4-(Dicyanomethylene)-2-methyl-6-(4-dimethylaminostyryl)-4H-pyran (DCM), which is 30% in methanol[1]. n_{DCM} and n_{sample} represent the refractive indices of the solvents of methanol and toluene. A_{DCM} and A_{sample} stand for the absorbance DCM and sample at the excitation wavelength. $[Area]_{sample}$ and $[Area]_{DCM}$ are the integrated areas of the photoluminescence of Eu{(+)-facam}$_3$ and DCM. The emission at 613 nm corresponds to the Eu{(+)-facam}$_3$ molecules. The trap state of CdS was subtracted and only the sharp emission from Eu^{3+} was used to compare the PLQY of Eu{(+)-facam}$_3$. The total absorption includes both CdS and Eu{(+)-facam}$_3$ contribution.

CdS	**Eu{(+)-facam}$_3$ PLQY**	
	Excite at 405 nm/ %	Excite at CdS band edge/ %
CdS 416nm	0.12	0.05
CdS 435nm	0.11	0.11
CdS 439nm	0.09	0.10
CdS 445nm	0.03	0.02

Table S3. Eu{(+)-facam}$_3$ PL enhancement with CdS and 1–NCA ligand calculated by Eq. S1. The PLQY error estimates is less than 0.01%.

2.4.4 Eu{(+)-facam}$_3$ PL measurements with CdSe 524nm and 9–ACA ligand

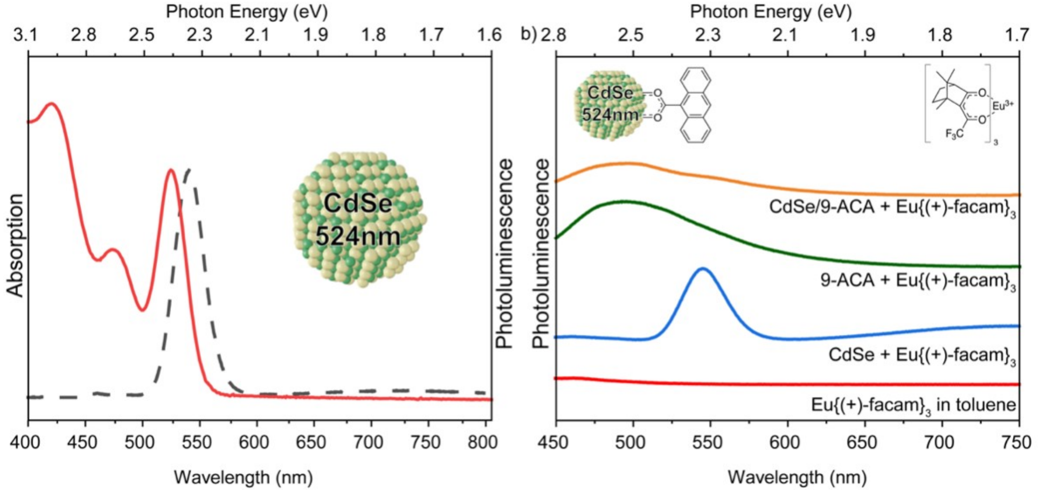

Figure S4. (a)The absorption of CdSe with absorption maxima of 524 nm (solid line) and photoluminescence spectra (dashed line), in toluene, RT. (b) With excitation at 405 nm, the photoluminescence spectra of 1.23 mM Eu{(+)-facam}$_3$ in different solutions, i.e. 524 nm CdSe/9–ACA (red), 1.91 mM 9–ACA in toluene (green), 524 nm CdSe only (blue) showed no enhancement of Eu(III) PL. The broad peak in green at around 470-500 nm is 9–ACA excimer emission.[2]

2.4.5 CdS/ZnS core shell

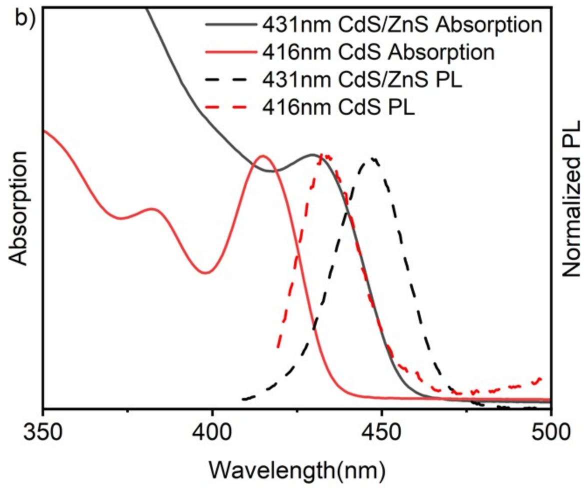

Figure S5. Absorption (solid line) of the 431 nm CdS/ZnS core/shell QDs with 3 monolayers of ZnS grown on 416 nm CdS QDs. The wavelengths are the absorption maxima of the nanoparticles. The normalized photoluminescence spectra with excitation at 405 nm are in the dashed line.

2.5 Ultrafast Transient Absorption Spectroscopy

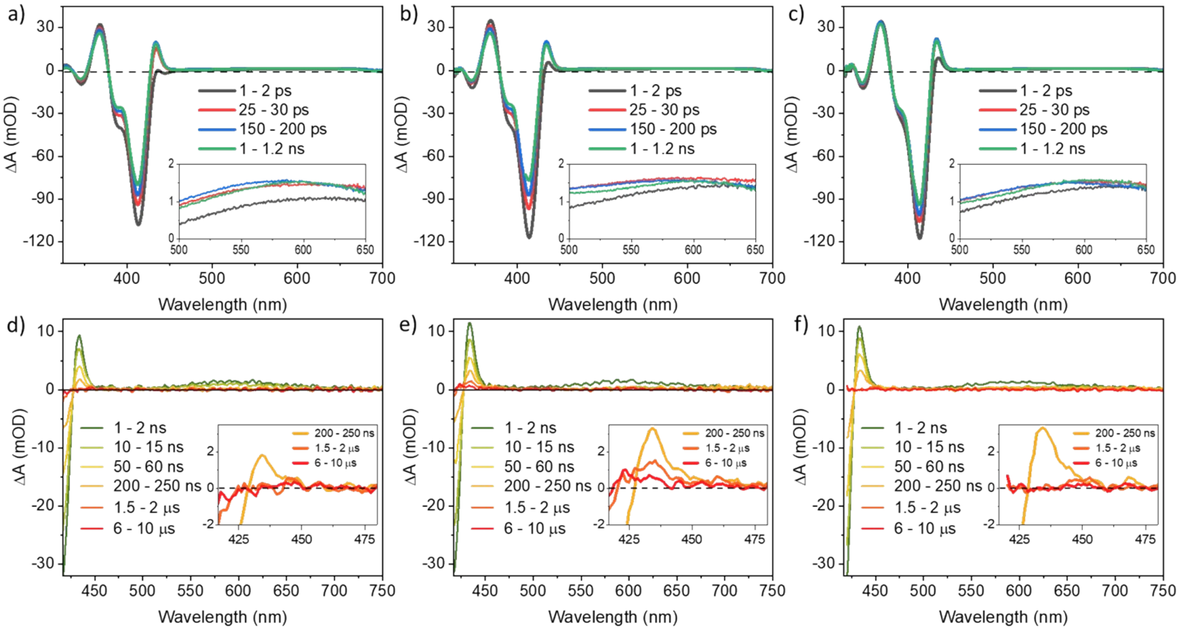

Figure S6. First row: picosecond TA spectra of a) CdS QDs, b) CdS/1–NCA, and c) CdS/1–NCA + Eu{(+)-facam}$_3$. Inset: a zoom-in view of the same spectra from 500 nm to 650 nm to show the photoinduced absorption of trapped hole. Second row: nanosecond TA spectra of d) CdS QDs, e) CdS/1–NCA, and f) CdS/1–NCA + Eu{(+)-facam}$_3$. Inset: a zoom-in view of the same spectra from 417 nm to 480 nm to compare the Stark effect induced PA signal in pure CdS QD and the absorption of ^{3}NCA*.

The TA spectra in the picosecond time window were measured with such excitation that the average number of excitons per CdS QD $\langle N_X \rangle$ is 0.93. $\langle N_X \rangle$ at delay time *t* is estimated by equation S2.

$$\langle N_X \rangle(t) = \frac{2\Delta A(t)}{A} \qquad (Eq\ S2)$$

In equation S2, $\Delta A(t)$ is the exciton bleach (XB) amplitude at delay time *t*. The factor 2 represents the double degeneracy of the $1S_e$ level at the conduction band edge. Note that hole contribution to XB is omitted here assuming ultrafast hole trapping in the CdS QDs.

This high pump fluence was required to clearly observe the photoinduced absorption (PA) of trapped hole. Figure S6a-c show that, except the initial fast Auger recombination of biexcitons (< 30 ps), both the XB and trapped hole PA signal show negligible decay within 1 ns in all the three samples. Thus, the discussion of TA results will focus on delay times longer than 1 ns.

For the nanosecond TA experiments, the $\langle N_X \rangle$ is 0.34 at 1 ns. Note that only single exciton state survives after 1 ns due to the fast Auger combination of biexcitons. As shown below, hole transfer and ^{3}NCA* formation are both later than 1 ns. Therefore, the initial biexciton state under this high pump fluence has no impact on the study of the QD-to-1–NCA TET.

As shown in the inset of Figure S6 (d) and (e), ^{3}NCA* signal is at the same position as the Stark effect signal but lives longer. In inset of Figure S6 (f), negligible ^{3}NCA* signal shows up in the spectra averaged from 1.5 μs to 2 μs and 6 μs to 10 μs. However, the 200 ns to 250 ns spectrum shows higher and broader positive peak from 425 nm to 450 nm compared to pure QD. This may be caused by a short-lived ^{3}NCA* signal overlapping with the Stark effect PA signal in CdS/1–NCA + Eu{(+)-facam}$_3$.

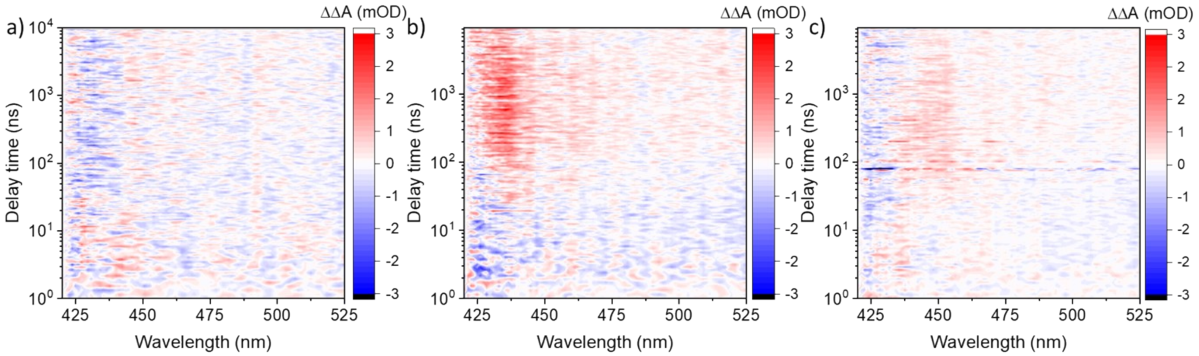

Figure S7. Double difference TA spectra of a) CdS QDs, b) CdS/1–NCA, and c) CdS/1–NCA + Eu{(+)-facam}$_3$.

To clearly show the ^{3}NCA* spectrum and kinetics, the overlapped CdS QD signal in CdS/1–NCA and CdS/1–NCA + Eu{(+)-facam}$_3$ was subtracted. It is assumed that i) from 1 ns to 2 ns, no ^{3}NCA* forms and the CdS QD signal dominates the TA spectra; ii) at any delay time, the signal from 420 nm to 422 nm is only contributed by the XB of CdS QDs. Thus, for each sample, the TA spectrum averaged from 1 ns to 2 ns was taken as the reference spectrum, $\Delta A(\lambda, 1{\sim}2\ ns)$, to represent the CdS QD TA signal. Then, at each delay time, the reference spectrum was scaled and subtracted from the original spectrum to remove the QD component. The scaling factor $\gamma(t)$ ensures that the scaled QD spectrum and the original spectrum have the same XB amplitude from 420 nm to 422 nm, so that only the QD component will be subtracted. $\gamma(t)$ is calculated as in equation S3. This procedure results in the double difference TA spectrum, $\Delta\Delta A(\lambda,t)$, as shown in equation S4.

$$\gamma(t) = \frac{\Delta A(420{\sim}422\ nm,t)}{\Delta A(420{\sim}422\ nm,\ 1{\sim}2\ ns)} \qquad (EqS3)$$

$$\Delta\Delta A(\lambda,t) = \Delta A(\lambda,t) - \gamma(t) \times \Delta A(\lambda,\ 1{\sim}2\ ns) \qquad (EqS4)$$

The double difference TA spectrum of CdS/1–NCA and CdS/1–NCA + Eu{(+)-facam}$_3$ clearly show the positive TA signal of ^{3}NCA* from 425 nm to 450 nm. The kinetics of ^{3}NCA* were then obtained by averaging the kinetics around 440 nm in the $\Delta\Delta A(\lambda,t)$ data, as shown in Figure 4 and Figure S9. On the other hand, the same procedure applied to the CdS QD sample (Figure S7a) shows no such positive signal, validating the above assumptions and the existence of the ^{3}NCA* in the other two samples.

3. TA kinetics fitting.

Figure S8 shows the excited state dynamics in CdS/1–NCA. Since the trapped hole and conduction band electron show TA signals at different positions and their dynamics are well separated in time domain according to the hole transfer mediated TET mechanism discussed in the main text, their kinetics fitting is treated separately, as shown in Figure S8b and S8c.

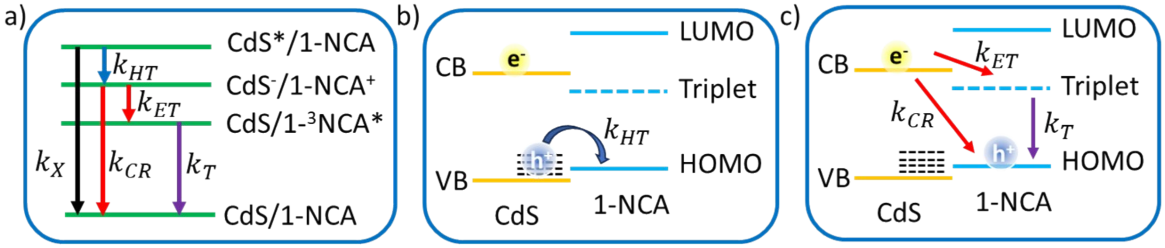

Figure S8. Schematic of excited state dynamics in CdS/1–NCA. a) State representation of the CdS/1–NCA sample. The excited CdS QD can decay through intrinsic decay pathway (k_X) to the ground state or hole transfer (k_{HT}) to the charge separated state. The charge separated state can then decay through electron transfer (k_{ET}) to form ^{3}NCA* or charge recombination (k_{CR}) to form the ground state. The ^{3}NCA* decays with rate constant k_T. b) Schematic of trapped hole transfer in the single particle representation. c) Schematic of the electron dynamics. These dynamics can be separated with the hole transfer due to its slow rate constants k_{ET} and k_{CR} compared to k_{HT}.

3.1 Trapped hole transfer kinetics.

The trapped hole kinetics in pure CdS QDs is fitted to a two-exponential decay function, as shown in equation S5, where $A_{t,0}$ is the total amplitude, $k_{t,i}$ and a_i are the intrinsic decay rate constant of trapped hole and related relative amplitude. Note that the second exponential decay accounts for the observed long-lived tail as shown in Figure 4a. The origin of this long-lived part is unclear as it is not affected by hole transfer. ~~Thus, this part is not considered in the following fitting of hole transfer.~~ In CdS/1–NCA and CdS/1–NCA + Eu{(+)-facam}$_3$, the short-lived part of the trapped hole decay is accelerated by hole transfer, while the long-lived tail is the same as in pure QD. The fitting function is given by equation S6, where the rate constant of the first exponential decay term is increased by k_{HT} to represent hole transfer, and the second exponential decay term is the same as in equation S5. Equation S5 and S6 are globally fitted to the trapped hole kinetics in all three samples with shared rate constants. The fitting parameters are listed in Table S3 and the fitting curves as shown in Figure 4a and Figure S9. The hole transfer efficiency is estimated by equation S7.

$$A_{t,QD}(t) = A_{t,0}\sum_{i=1}^{2} a_i e^{-k_{t,i}t} \qquad (Eq\ S5)$$

$$A_{t,QD-NCA}(t) = A_{t,QD-NCA-Eu}(t) = A_{t,0}\left(a_1 e^{-(k_{t,1}+k_{HT})t} + a_2 e^{-k_{t,2}t}\right) \qquad (Eq\ S6)$$

$$\phi_{HT} = \frac{k_{HT}}{k_{t,1}+k_{HT}} \qquad (Eq\ S7)$$

a_1/%	$k_{t,1}$/ns^{-1}	a_2/%	$k_{t,2}$/μs^{-1}	k_{HT}/ns^{-1}	φ_{HT}/%
87.8 ± 1.0	0.039 ± 0.001	12.2 ± 1.0	0.156 ± 0.024	0.111 ± 0.005	74.1 ± 1.1

Table S3. Fitting parameters for the trapped hole transfer kinetics.

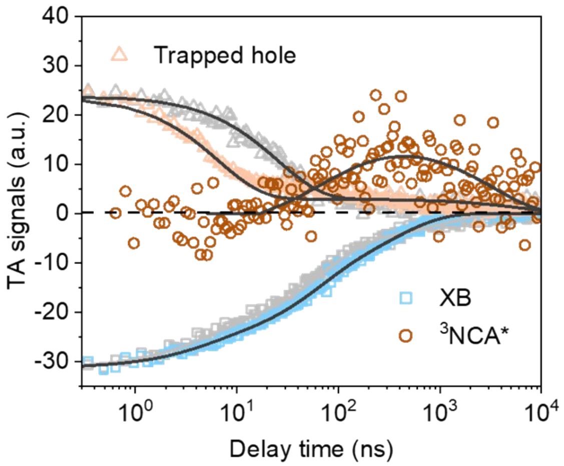

Figure S9. Fitting results of the trapped hole (light orange triangles), XB (cyan squares) and ^{3}NCA* (dark yellow circles) kinetics in CdS/1–NCA + Eu{(+)-facam}$_3$. The trapped hole (grey triangles) and XB (grey squares) in pure CdS QDs are also shown for comparison. Solid lines represent the fitting curves. Note that the amplitudes of the kinetics are scaled for better comparison.

3.2 Electron transfer and triplet kinetics fitting.

The electron dynamics is followed by the CdS XB signal. In pure CdS QDs, the XB kinetics is found to be best fit by a three-exponential decay function, as shown in equation S8, where $A_{XB,0}$ is the total XB amplitude, $k_{X,i}$ and a_i are the intrinsic exciton or electron decay rate constant and related relative amplitude. The necessity for three exponential decays indicates that there may be three sub populations in the QD ensemble with different properties.

$$A_{XB,QD}(t) = A_{XB,0}\sum_{i=1}^{3} a_i e^{-k_{X,i}t} \qquad (Eq\ S8)$$

In CdS/1–NCA, part of the complexes (with percentage b_1) are in the charge separated state, where the electron transfer to 1-NCA$^+$ through two competitive pathways: to form the triplet with rate constant k_{ET}, and to form the ground state with rate constant k_{CR}, as shown in Figure S8c. It was found that only one k_{ET} is needed for the three sub populations of the QDs. In the other part (with percentage b_2), the electron recombines with the hole in the QD. Equation S9 is used to fit the XB decay kinetics. Note that a single exponential decay function for the b_2 part was found to fit the data best, rather than the three-exponential decay function.

$$A_{XB,QD-NCA(-Eu)}(t) = A_{XB,0}\left(b_1\sum_{i=1}^{3} a_i e^{-(k_{CR,i}+k_{ET})t} + b_2 e^{-k_X^{'}t}\right) \qquad (Eq\ S9)$$

The ^{3}NCA* kinetics was fit to equation S10 according to the model in Figure S8c. The first exponential function in the parentheses represents the decay of ^{3}NCA* with rate constant k_T, and the second exponential function represent the growth kinetics, which is coupled with the decay of the conduction band electron. ε' represents the extinction coefficient ratio between the CdS 1S exciton bleach and the ^{3}NCA* T_1-to-T_n absorptions, together with the scaling factor of the kinetics data in Figure 4 and S9.

$$A_{T,QD-NCA(-Eu)}(t) = \varepsilon' b_1 A_{XB,0}\sum_{i=1}^{3} a_i \frac{k_{ET}}{k_{CR,i}+k_{ET}-k_T}\left(e^{-k_T t} - e^{-(k_{CR,i}+k_{ET})t}\right) \qquad (Eq\ 10)$$

Equation S9 and S10 are globally fitted to the data in both CdS/1–NCA or CdS/1–NCA + Eu{(+)-facam}$_3$ with shared k_{ET} and $k_{CR,i}$ but different b_i and k_T. The fitting curves are shown in Figure 4 and Figure S9. Fitting parameters are summarized in Table S4.

	QD	QD-NCA	QD-NCA-Eu
$A_{XB,0}$/mOD	31.6		
a_1/%	23.4 ± 1.7		
$k_{X,1}(k_{CR,1})$/ns^{-1}	0.233 ± 0.038		
a_2/%	57.1 ± 1.6		
$k_{X,2}(k_{CR,2})$/μs^{-1}	14.8 ± 1.0		
a_3/%	19.4 ± 1.4		
$k_{X,3}(k_{CR,3})$/μs^{-1}	0.994 ± 0.116		
b_1/%		88.7 ± 3.5	68.5 ± 3.8
k_{ET}/μs^{-1}		4.86 ± 0.94	
b_2/%		11.3 ± 3.5	31.5 ± 3.8
k_X'/μs^{-1}		1.33 ± 0.74	2.23 ± 0.46
ε'		1.68 ± 0.16	2.00 ± 0.22

k_T/ms^{-1}		99.5 ± 17.3	291.8 ± 42.4

Table S4. Fitting parameters of the XB kinetics in CdS QDs, CdS/1–NCA, and CdS/1–NCA + Eu{(+)-facam}$_3$.

Since $k_{CR,i}$ and k_{ET} are mostly indistinguishable in the fitting, $k_{CR,i}$ are set the same as $k_{X,i}$, as they both describe the decay of the conduction band electron with a localized hole in surface traps or surface adsorbed 1–NCA molecules. However, as discussed in the main text, the high QD-to-1–NCA TET efficiency in CdS/1–NCA implies that k_{ET} may outcompete $k_{CR,i}$.

The fitting results also explain the small difference between the XB kinetics in Figure 4a and Figure S9. The extra electron decay rate constant (k_{ET}, 4.86 ± 0.94 μs^{-1}) induced by 1-NCA is smaller than the major electron decay rate constant in pure CdS ($k_{X,1}$, 0.233 ± 0.038 ns^{-1}, and $k_{X,2}$, 14.8 ± 1.0 μs^{-1}), so the XB kinetics change is small. Note that in Figure S9, the CdS/1–NCA + Eu{(+)-facam}$_3$ XB kinetics shows slightly slower decay than pure CdS within 500 ns, which may be caused by other minor QD subpopulations with slower XB decay kinetics in this sample that was not resolved in the fitting model. This may also explain why the three-exponential decay function used for pure QD cannot fit the b_2 part in equation S9.

The average ^{3}NCA* formation rate constant is calculated as in equation S11.

$$\langle k_{T,formation}\rangle = \sum_{i=1}^{3} a_i\left(k_{CR,i} + k_{ET}\right) \qquad (Eq\,S11)$$

The TET efficiency from 1–NCA to Eu{(+)-facam}$_3$ is estimated through the ^{3}NCA* decay rate constant k_T, as shown in equation S12. It is assumed that in the presence of Eu{(+)-facam}$_3$, the only extra decay pathway of ^{3}NCA* is TET to Eu{(+)-facam}$_3$. Thus, the rate constant of this TET step is the change of the ^{3}NCA* decay rate constant: $k_{T,QD-NCA-Eu} - k_{T,QD-NCA} = 192.3 \pm 45.8\,ms^{-1}$.

$$\phi_{TET,NCA-to-Eu} = 1 - \frac{k_{T,QD-NCA}}{k_{T,QD-NCA-Eu}} = 65.9 \pm 7.7\% \qquad (Eq\,S12)$$

4. Estimation of QD-to-1–NCA TET efficiency.

The QD-to-1–NCA TET efficiency was estimated using equation S13.

$$\phi_{TET,QD-to-NCA} = \frac{\Delta A_{NCA}/\varepsilon_{NCA}}{2\Delta A_{QD}/\varepsilon_{QD}} \qquad (Eq\,S13)$$

In equation S13, ΔA_{NCA} is the maximum absorbance of ^{3}NCA*. For CdS/1–NCA, ΔA_{NCA} is taken from the $\Delta\Delta A$ spectrum (Figure S7b) averaged from 0.4 μs to 0.8 μs. For CdS/1–NCA + Eu{(+)-facam}$_3$, ΔA_{NCA} is taken as the averaged $\Delta\Delta A$ spectrum (Figrue S6c) from 0.3 μs to 0.6 μs. The spectra are shown in Figure S10. The blank spectrum of pure CdS QDs averaged at corresponding delay times are subtracted in these two spectra. ΔA_{NCA} is taken from the peak value. ΔA_{QD} is the XB peak amplitude at 1 ns. The factor 2 accounts for the double degeneracy of the 1S$_e$ level in CdS QDs. ε_{NCA} is the extinction coefficient of the ^{3}NCA* at 425 nm, 13200 M^{-1}cm^{-1}. Note that the ^{3}NCA* absorption in Figure S10 is red shifted compared to literature,[3] which may be caused by different local dielectric environment on the QD surface. ε_{QD} is the 1S exciton extinction coefficient of the CdS QD, 501069 M^{-1}cm^{-1}, calculated according to literature.[4] The calculated $\phi_{TET,QD-to-NCA}$ values are listed in Table S5.

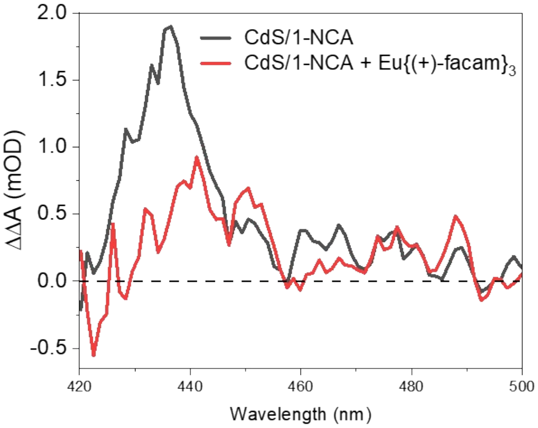

Figure S10. 3NCA* spectra of the maximum amplitude in CdS/1–NCA (black) and CdS/1–NCA + Eu{(+)-facam}$_3$ (red).

	ΔA_{NCA}/mOD	ΔA_{QD}/mOD	$\varphi_{TET,QD\text{-}to\text{-}NCA}$/%
CdS/1–NCA	1.90	48.4	74.4
CdS/1–NCA + Eu{(+)-facam}$_3$	0.93	49.2	35.8

Table S5. Values used in the calculation of $\phi_{TET,QD-to-NCA}$.

$\phi_{TET,QD-to-NCA}$ is smaller for CdS/1–NCA + Eu{(+)-facam}$_3$, probably due to the extra decay pathway of TET to Eu{(+)-facam}$_3$, which decreases the maximum value of ΔA_{NCA}.

Reference

1. Ravi Kumar, K.; Satyen, S.; Manjeev, S.; Akhila, M., Photophysical Properties of 4-(Dicyanomethylene)-2-Methyl-6-(4-Dimethylaminostyryl)-4H-Pyran (DCM) and Optical Sensing Applications. In *Photophysics, Photochemical and Substitution Reactions*, Satyen, S.; Ravi Kumar, K.; Tanja, V. S., Eds. IntechOpen: Rijeka, 2020; p Ch. 1.
2. Jaramillo-González, C.; Morales Cueto, R.; Rodríguez-Córdoba, W., Absorption and Emission Spectra of Anthracene-9-Carboxylic Acid in Solution Within the Polarizable Continuum Model. In *Concepts of Mathematical Physics in Chemistry: A Tribute to Frank E. Harris - Part B*, 2016; pp 61-94.
3. Luo, X.; Han, Y.; Chen, Z.; Li, Y.; Liang, G.; Liu, X.; Ding, T.; Nie, C.; Wang, M.; Castellano, F. N.; Wu, K., Mechanisms of Triplet Energy Transfer Across the Inorganic Nanocrystal/Organic Molecule Interface. *Nat Commun* **2020,** *11* (1), 28.
4. Yu, W. W.; Qu, L.; Guo, W.; Peng, X., Experimental Determination of the Extinction Coefficient of CdTe, CdSe, and CdS Nanocrystals. *Chemistry of Materials* **2003,** *15* (14), 2854-2860.